China Ocean Eng., 2022, Vol. 36, No. 2, P. 311–321
DOI: https://doi.org/10.1007/s13344-022-0027-6, ISSN 0890-5487
http://www.chinaoceanengin.cn/ E-mail: coe@nhri.cn

Adaptive Controller Design for Dynamic Maneuvers of High Speed Underwater Vehicles

Bui Duc Hong PHUC[a], Sam-Sang YOU[b, *], Phuc Thinh DOAN[c], Sang-Do LEE[d]

[a] Department of Mechanical Engineering, The University of Tulsa, Tulsa, OK 74104, USA

[b] Division of Mechanical Engineering, Korea Maritime and Ocean University, Busan 49112, Republic of Korea

[c] Institute of Interdisciplinary Social Sciences, Nguyen Tat Thanh University, Ho Chi Minh City, Vietnam

[d] Division of Navigation and Information System, Mokpo National Maritime University, Mokpo, Jeollanam-do 58628, Republic of Korea

Received January 31, 2021; revised December 7, 2021; accepted January 12, 2022

Abstract

The control synthesis of the high-speed underwater vehicle faces many technical challenges due to its inherent structure and surrounding operational environment. In this paper, the dynamical behavior is firstly described through a bifurcation analysis to give some insights for robust control synthesis. Then a novel adaptive fractional-order sliding mode controller (AFOSMC) is realized to effectively manipulate the supercavitating vehicle against payload changes, nonlinear planing force, and external disturbances. The fractional order (FO) calculus can offer more flexibility and more freedom for tuning active control synthesis than the integer-order counterpart. In addition, the adaptation law has been presented to directly handle the payload change effects. The stability of the controlled vehicle system is proven via Lyapunov stability theory. Next, the dynamic performance of the proposed controller is verified through extensive simulation results, which demonstrate the control accuracy with faster responses compared with existing integer-order controllers. Finally, the proposed fractional order controllers can provide higher performance than their integer order counterparts with control algorithms.

Key words: fractional order calculus, supercavitating, underwater vehicles, planing force, payload change, adaptive sliding mode control

Citation: Phuc, B. D. H., You, S. S., Doan, P. T., Lee, S. D., 2022. Adaptive controller design for dynamic maneuvers of high speed underwater vehicles. China Ocean Eng., 36(2): 311–321, doi: https://doi.org/10.1007/s13344-022-0027-6

1 Introduction

There has been a growing interest in developing control system design for autonomous underwater vehicles (AUVs) with time-varying parameters and unmodelled dynamics (You, et al., 2011; Zhao, et al., 2019). The speed of traditional underwater vehicle is limited by intense skin friction drag on the hull of the surrounding fluid with multiphase flow. Recently, high speed underwater bodies have overcome the design limitation imposed by fluid dynamics with supercavitation technology. Then, the speed of a supercavitating vehicle can be extremely increased with respect to conventional underwater vehicle. In order to exploit this emerging technology with proper design, a supercavitating vehicle must be implemented with a sharp-edge cavitator at its nose (Mao and Wang, 2009) which can provide rotation around an axis. When the supercavitating body is moving at an extremely high speed, the cavitator causes local pressure drops to form low-density gaseous cavities. If a single gaseous cavity is maintained big enough to envelop most of the rapid vehicle body, except control surfaces such as the cavitator and the elevators, the hydrodynamic drag is dramatically reduced and the underwater vehicle can achieve very high speed (Jafarian and Pishevar, 2016). A developmental technology will give undersea vehicle with new capabilities in speed and maneuverability.

The dynamic models of supercavitating vehicles have been reported in many papers (May, 1975; Rand et al., 1997; Kulkarni and Pratap, 2000; Dzielski and Kurdila, 2003). One of the well-known models is the one proposed by Dzielski and Kurdila (2003) which has four state variables to describe the dive-plane dynamics. As illustrated in Fig. 1, this model is well defined and is suitable for the control synthesis. In fact, the uncontrolled dynamics of this rapid vehicle is highly unstable. Even though a linear-feedback controller was proposed in their research, it could not smoothly stabilize the underwater vehicle and its dynamical behavior clearly shows oscillatory motions. There have been several papers investigating the bifurcation behavior of the

*Corresponding author. E-mail: ssyou@kmou.ac.kr

vehicle. Most of them studied the bifurcation in term of the cavitation number to give stability analysis. However, there is almost no paper working on the bifurcation behavior that considers the vehicle mass change. It is noteworthy that the vehicle weight and the planning force can be major causes of the dynamic instability (Mao and Wang, 2009). In this paper, the bifurcation analysis is performed respecting to the vehicle mass variations to explain the stability issue and to suggest a more suitable vehicle design.

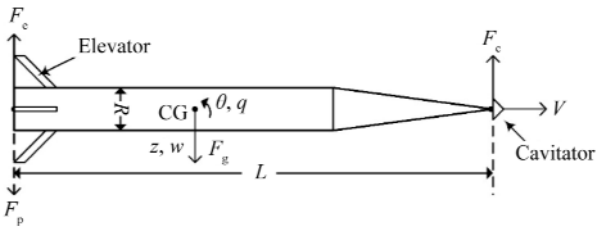

Fig. 1. A simplified vehicle configuration with reference frame.

Robust control synthesis can solve various challenges for high speed vehicle design. The vehicle controller should deal with not only its highly unstable structure, but also many other factors such as insufficient lift force, highly coupled dynamics, and model uncertainties. Those are mainly caused by hydrodynamic effects, nonlinear forces, and unpredictable external disturbances (Kirschner et al., 2002). Besides control robustness, due to the high-speed maneuver, the vehicle dynamics should be regulated with fast transient performance with accuracy while minimizing any possible overshoot or undershoot. Thus, control synthesis will be one of the most challenging parts in a complete supercavitating vehicle design. There have been various control methods presented for the supercavitating vehicle dynamics ranging from simple to advanced schemes, such as receding horizon control (Vanek et al., 2007), switch control (Lin et al., 2008), sliding mode controller (SMC) (Mao and Wang, 2009; Lv et al., 2010, 2011; Fan et al., 2010; Zhao et al., 2011), adaptive control (Mao and Wang, 2015), model predictive control (Fan et al., 2011), backstepping control (Lin et al., 2006; Han et al., 2010), linear parameter varying control (Mao and Wang, 2009; Vanek et al., 2010), robust control (Mao and Wang, 2009; Anukul, 2005), and μ control (Zhao et al., 2014). Among the existing controllers, SMC strategy is particularly considered as high applicability in undersea reality against uncertainties (Utkin, 2008).

The control requirements of the high-speed supercavitating vehicle include fast transient response with ensuring small overshoots as well as settling time, and high robustness to disturbances with no chattering. Owing to those requirements, the underwater vehicle needs a robust controller against disruptions. In this paper, a new AFOSMC is proposed to regulate the vehicle robustly as well as to gain more flexibility in dealing with uncertainties. AFOSMC scheme is realized by SMC based on fractional-order calculus (FOC) instead of an integer-order SMC. In fact, FOC is a branch of mathematical analysis that extends derivatives and integral to an arbitrary order so that it can provide better descriptions of diverse nonlinear phenomena. Furthermore, it provides a greater degree of freedom for dynamical behavior and flexibility for control synthesis. Nowadays, most of the fractional-order controllers utilize simple proportional-integral-derivative (PID) algorithm (Podlubny et al., 1997; Podlubny, 1999; Xue and Chen, 2002) or CRONE algorithm (Oustaloup et al., 2000a, 2000b) due to their sufficient supporting algorithms. In addition to FOC strategy, the proposed controller contains adaptation scheme. The adaptive control can update their parameters to effectively react to external disturbances as well as vehicle's inherent varying factors such as nonlinear planing force or payload changes. The extensive simulation results show that the proposed AFOSMC provides good transient responses as well as high robustness in dealing with external disruptions while eliminating most of the uncertainty effects. Finally, the obtained results show that the proposed control algorithm outperformed super-twisting sliding mode controller (STWSMC) as well as the other existing controllers in the literature.

2 Vehicle dynamics and qualitative behaviors

As illustrated in Fig. 1, the dive-plane motions of a supercavitating vehicle are described with a body-fixed reference frame. In this reference frame, the origin is located at the center of gravity (CG), the x-axis is along the vehicle axis of symmetry, the y-axis points to the starboard, and the z-axis points downwards. The four state variables for the vehicle model include the vertical position z, the vertical speed w, the pitch angle θ and the pitch rate q. The dynamical behaviour of the supercavitating vehicle is controlled through the deflections of the elevator angle δ_e in the aft and the cavitator deflection angle δ_c in the front part. The vehicle is assumed to move forward with a constant speed, V, where L is the vehicle length and R is the body radius. There are totally four forces acting on the underwater vehicle body, including two lift forces by the cavitators and elevators, the gravity force F_g and the planing force F_p which is not always present. By applying Newton-Euler formulation, the nonlinear differential equations describing vertical vehicle dynamics can be written in the compact state-space form as follows (Han and Geng, 2012):

$$\dot{\boldsymbol{x}} = \boldsymbol{A}\boldsymbol{x} + \boldsymbol{B}\boldsymbol{u} + \boldsymbol{G} + \boldsymbol{F}. \tag{1}$$

In this representation, the vector of state variables is described as $\boldsymbol{x}$ ($\in \Re^4$) and the control input vector is represented as $\boldsymbol{u}$ ($\in \Re^2$),

$$\begin{aligned} &\boldsymbol{x} = [z \quad w \quad \theta \quad q]^{\mathrm{T}}; \\ &\boldsymbol{u} = [u_1 \quad u_2]^{\mathrm{T}} = [\delta_e \quad \delta_c]^{\mathrm{T}} \end{aligned} \tag{2}$$

and the system matrices and vectors are given as:

$$\boldsymbol{A}=\begin{bmatrix} 0 & 1 & -V & 0 \\ 0 & a_{22} & 0 & a_{24} \\ 0 & 0 & 0 & 1 \\ 0 & a_{42} & 0 & a_{44} \end{bmatrix},\ \boldsymbol{B}=\begin{bmatrix} 0 & 0 \\ b_{21} & b_{22} \\ 0 & 0 \\ b_{41} & b_{42} \end{bmatrix} \tag{3}$$

$$\boldsymbol{G}=[0 \quad F_{\mathrm{g}} \quad 0 \quad 0]^{\mathrm{T}},\ \boldsymbol{F}=[0 \quad d_2F_{\mathrm{p}} \quad 0 \quad d_4F_{\mathrm{p}}]^{\mathrm{T}}. \tag{4}$$

The detailed elements of A, B, G, and F are clearly given in Appendix A. The interested readers can refer to some references (Dzielski and Kurdila, 2003; Han and Geng, 2012; Phuc et al., 2019) for further details. For the dynamical analysis and control synthesis, the related vehicle parameters are also described in Table 2 in Appendix B.

It is worth noting that the vehicle dynamics in Eq. (1) is particularly suffered from planing force F_{p} which is not well understood yet. The main difficulty comes from the complex nonlinear interaction among solid body, sea water, and gaseous phase, in which its identification is of great importance. This force typically occurs in a nonlinear discontinuous manner, and exists only if the magnitude of the vertical velocity w is larger than a certain value w_{o}, where the vehicle aft end pierces the supercavity and contacts with water. Once occurred, it has the tendency of pushing the vehicle aft end toward the center of the supercavity. If the magnitude of the planing force is too high, the vehicle tail will be over-pushed to the opposite side of the supercavity and the planing force on the other side will occur. This repeating process is the so-called tail-slap phenomenon, which is one of the main sources for the vehicle instability, making the control design and maneuvering more difficult. Assume that the vehicle body has a uniform density $\rho_{\mathrm{b}}=m\rho$, where the relative density m is compared with that of the surrounding water ρ. It can be observed from Appendix A that the relative density m is the main constituent of vehicle mass and moment of inertia. Note that the vehicle mass M is calculated by (Dzielski and Kurdila, 2003)

$$M=\frac{7}{9}m\rho\pi R^2L, \tag{5}$$

where L is the vehicle body length and R denotes its radius. In order to analyze the effects or variation of relative density m on the vehicle mass and inertia as well as the whole vehicle dynamics, by letting $K_M=\frac{7}{9}\rho\pi R^2L$, it is known as:

$$M=mK_M, \tag{6}$$

while the moment of inertia I_{yy} is given as:

$$I_{yy}=\frac{11}{60}R^4Lm\rho\pi+\frac{1933}{45360}R^2L^3m\rho\pi. \tag{7}$$

By letting $K_\theta=\frac{11}{60}R^4L\rho\pi+\frac{1933}{45360}R^2L^3\rho\pi$, it can be described by

$$I_{yy}=mK_\theta. \tag{8}$$

During vehicle maneuvering, its mass can be reduced due to fuel consumption; or the payload which contributes to the whole vehicle mass may vary in each launch. According to Eq. (5), the vehicle mass changes will occur when the relative density m changes. When m is varying, it will affect both system matrices $\boldsymbol{A}$ and $\boldsymbol{B}$ as described in Appendix A (details are given in Eqs. (A1) and (A2)). Note that the free system has no equilibria and could be highly unstable. The basic control attempt in the original work has been realized by a state feedback control law which can keep the vehicle stable from instability (Phuc et al., 2020). However, the state feedback controller cannot completely eliminate the planing force, which still has a strong effect on vehicle dynamics. By investigating dynamical behaviors respecting to its mass change, a bifurcation diagram is illustrated in Fig. 2. Based on the original work with the vehicle mass of about 23 kg, there are bifurcations in its vertical velocity w, according to the stability analysis. While w is the main factor that causes the planing force, this stability analysis leads to bifurcating planing force and may cause the periodic motion. From the bifurcation analysis, the underwater vehicle is designed with the total mass in the range from 25 kg to 27 kg, which will obviously produce no bifurcation.

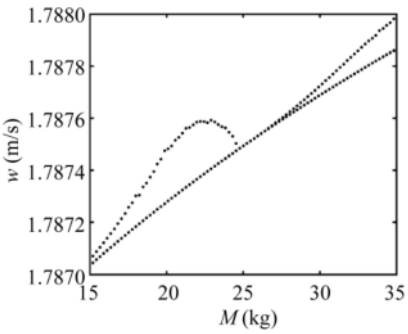

Fig. 2. Bifurcation diagram of the supercavitating vehicle as its mass change.

Besides the nonlinear planing force and uncertain mass, the undersea maneuvering of the supercavitating vehicle will also face another significant challenge which is the external disturbance. Since the vehicle operates in underwater environment, the disturbances can be described in currents, obstacles or salinity. Therefore, an active robust controller is always necessary to stabilize the vehicle dynamics while providing accurate vehicle maneuver against undersea environmental uncertainty. A novel controller should be implemented for the supercavitating vehicles to ensure robust performance and stability against the payload effect, planing force and external disturbance.

3 Control synthesis for underwater vehicles

3.1 Fraction order calculus

Fractional order calculus provides control system to enhance the overall performance including dynamical behavi-

or, safety, stability, and flexibility for realization. For the control synthesis, the fractional order α can be an arbitrary complex number. In fact, fractional order calculus is a generalization of integration and differentiation to non-integer order operator ${}_a\mathrm{D}_t^{\alpha}$ defined as follows (Oustaloup et al., 2000b):

$$ {}_a\mathrm{D}_t^{\alpha}=\begin{cases}\dfrac{\mathrm{d}^{\alpha}}{\mathrm{d}t^{\alpha}}, & \mathrm{Re}(\alpha)>0\\ 1, & \mathrm{Re}(\alpha)=0\\ \displaystyle\int_a^t(\mathrm{d}\tau)^{-\alpha} & \mathrm{Re}(\alpha)<0\end{cases} \tag{9}$$

where $\mathrm{Re}(\alpha)>0$ corresponds to differentiators while $\mathrm{Re}(\alpha)<0$ yields integrators; a and t are the boundaries. In this study, the fractional order α is assumed to be real number ($\alpha\in\Re^+$) for simplicity. There are various types of definition for the fractional derivative of arbitrary order. There are some definitions for the general fractional operator, in which the common ones include Caputo and Riemann-Liouville definition. They are given as follows, respectively

$$ {}_a\mathrm{D}_t^{\beta}f(t)=\frac{1}{\Gamma(n-\beta)}\int_a^t\frac{f^{(n)}(\zeta)}{(t-\zeta)^{\beta-n+1}}\mathrm{d}\zeta; \tag{10}$$

$$ {}_a\mathrm{D}_t^{\beta}f(t)=\left(\frac{\mathrm{d}}{\mathrm{d}t}\right)^n\frac{1}{\Gamma(n-\beta)}\int_a^t\frac{f^{(n)}(\zeta)}{(t-\zeta)^{\beta-n+1}}\mathrm{d}\zeta, \tag{11}$$

where $n-1\leqslant\beta\leqslant n$; n is the smallest integer that is equal to or larger than β. Here by using β, which is non-integer order, the mathematical model can possibly capture more dynamics of the underwater vehicle system. Γ is the Gamma function defined as $\Gamma(n)=\int_0^{\infty}t^{n-1}\mathrm{e}^{-t}\mathrm{d}t$. It is noted that the difference between the two definitions is in the order of evaluation. In this paper, the Oustaloup recursive algorithm is implemented to approximate the fractional orders by classical integer order. More details of Oustaloup recursive approximation technique can be found in the work of Podlubny (1999).

3.2 Adaptive fractional order sliding mode control

The robustness of the supercavitating vehicle requests the control system to effectively deal with the planing force, payload changes, and external disturbance. Depending on its robust level and applicability, SMC strategy is chosen to combine with adaptive terms to directly adjust the control parameters to the changes in vehicle mass during the operation or in each launch. The fractional calculus can be realized to enhance the flexibility and effectiveness of the control scheme. Since the underwater vehicle is maneuvering in vertical plane, the actual feedback signals of z and θ should track the desired signals z_{d} and θ_{d}, respectively. Thus, tracking errors are defined as:

$$ \boldsymbol{e}=\begin{bmatrix}e_1\\e_2\end{bmatrix}=\begin{bmatrix}z-z_{\mathrm{d}}\\\theta-\theta_{\mathrm{d}}\end{bmatrix} \tag{12}$$

where e_1 and e_2 are the tracking errors for the vehicle's depth and pitch angle. For the control synthesis, the sliding variables are selected as

$$ \boldsymbol{s}=\begin{bmatrix}s_1\\s_2\end{bmatrix}=\begin{bmatrix}\dot{e}_1+\lambda_1e_1\\\dot{e}_2+\lambda_2e_2\end{bmatrix} \tag{13}$$

where the parameters λ_1 and λ_2 are real constants ($\in\Re$). The sliding surface is defined as:

$$ \boldsymbol{s}=\begin{bmatrix}\dot{z}-\dot{z}_{\mathrm{d}}+\lambda_1(z-z_{\mathrm{d}})\\\dot{\theta}-\dot{\theta}_{\mathrm{d}}+\lambda_2(\theta-\theta_{\mathrm{d}})\end{bmatrix}=\begin{bmatrix}0\\0\end{bmatrix} \tag{14}$$

where the gains (λ_1 and λ_2) are selected so that the solutions of the first order differential Eq. (14) exponentially converge to zero. Correspondingly, z and θ should track to the desired targets z_{d} and θ_{d} exponentially. A vehicle model from Eq. (1) is considered as an uncertain dynamical system. Since the planing force is typically not continuous with large magnitude, it will be considered as one of the leading disruptions to the vehicle maneuvers. This is mainly caused by strong nonlinear interaction of the high speed vehicle body and the cavity by multiphase flows. By replacing the term $\boldsymbol{F}$ by $\boldsymbol{\Phi}$ representing all uncertainties including external factors, planing forces and parameter variations, the perturbed nonlinear supercavitating vehicle dynamics in Eq. (1) can be modified as:

$$ \dot{\boldsymbol{x}}=\boldsymbol{A}\boldsymbol{x}+\boldsymbol{B}\boldsymbol{u}+\boldsymbol{G}+\boldsymbol{\Phi}. \tag{15}$$

In this formulation, the uncertainty term $\boldsymbol{\Phi}=\begin{bmatrix}\Phi_1 & 0 & \Phi_2 & 0\end{bmatrix}^{\mathrm{T}}$ is unknown but bounded as follows:

$$ |\boldsymbol{\Phi}(\boldsymbol{x},t)|\leqslant\boldsymbol{\Omega}, \tag{16}$$

where $\boldsymbol{\Omega}=\begin{bmatrix}\Omega_1 & 0 & \Omega_2 & 0\end{bmatrix}^{\mathrm{T}}$ is a vector of boundaries with each element ($\in\Re^+$).

By applying fractional order calculus, the time derivative of the sliding variables in Eq. (14) corresponding to the nominal vehicle system without disturbance term will be given by

$$ \dot{\boldsymbol{s}}=\begin{bmatrix}\dot{s}_1\\\dot{s}_2\end{bmatrix}=\begin{bmatrix}\dot{w}-V\dot{\theta}-\ddot{z}_{\mathrm{d}}+\lambda_1\dot{e}_1\\ \\ \dot{q}-\ddot{\theta}_{\mathrm{d}}+\lambda_2\dot{e}_2\end{bmatrix}= \begin{bmatrix}\dfrac{C_1-C_2}{mK_MV}w+\dfrac{C_1L_{\mathrm{c}}-C_2L_{\mathrm{e}}}{mK_MV}q+\dfrac{C_1}{mK_M}\delta_{\mathrm{e}}+\dfrac{C_2}{mK_M}\delta_{\mathrm{c}}+g-\\ Vq-\ddot{z}_{\mathrm{d}}+\lambda_{10}\mathrm{D}_t^{1-\beta}e_1\\ \dfrac{-C_1L_{\mathrm{c}}+C_2L_{\mathrm{e}}}{mK_{\theta}V}w+\dfrac{C_1L_{\mathrm{c}}^2-C_2L_{\mathrm{e}}^2}{mK_{\theta}V}q-\dfrac{C_1L_{\mathrm{c}}}{mK_{\theta}}\delta_{\mathrm{e}}-\dfrac{C_2L_{\mathrm{e}}}{mK_{\theta}}\delta_{\mathrm{c}}-\\ \ddot{\theta}_{\mathrm{d}}+\lambda_{20}\mathrm{D}_t^{1-\beta}e_2\end{bmatrix} \tag{17}$$

Then the control problem is equivalent to solving the finite-time stabilization of the following system:

$$ \dot{\boldsymbol{s}}=\boldsymbol{A}_{\boldsymbol{s}}+\boldsymbol{B}_{\boldsymbol{s}}\boldsymbol{u}, \tag{18}$$

where the feedback controller $\boldsymbol{u}$ includes an equivalent part and a reaching part. The controller $\boldsymbol{u}$ is introduced to drive the sliding variables to converge to zero as follows:

$$\boldsymbol{u} = [u_1 \quad u_2]^{\mathrm{T}} = \boldsymbol{\Lambda}\boldsymbol{B}_{\boldsymbol{s}}^{-1}[-\boldsymbol{A}_{\boldsymbol{s}} + \boldsymbol{u}_w], \tag{19}$$

where some matrices are given by

$$\boldsymbol{A}_{\boldsymbol{s}} = \begin{bmatrix} \dfrac{C_1 - C_2}{mK_M V} w + \dfrac{C_1 L_{\mathrm{c}} - C_2 L_{\mathrm{e}}}{mK_M V} q + g - Vq - \ddot{z}_{\mathrm{d}} + \lambda_{10} \mathrm{D}_t^{1-\beta} e_1 \\ \dfrac{-C_1 L_{\mathrm{c}} + C_2 L_{\mathrm{e}}}{mK_\theta V} w + \dfrac{C_1 L_{\mathrm{c}}^2 - C_2 L_{\mathrm{e}}^2}{mK_\theta V} q - \ddot{\theta}_{\mathrm{d}} + \lambda_{20} \mathrm{D}_t^{1-\beta} e_2 \end{bmatrix} \tag{20}$$

$$\boldsymbol{B}_{\boldsymbol{s}} = \begin{bmatrix} \dfrac{C_1}{mK_M} & \dfrac{C_2}{mK_M} \\ -\dfrac{C_1 L_{\mathrm{c}}}{mK_\theta} & -\dfrac{C_2 L_{\mathrm{e}}}{mK_\theta} \end{bmatrix} \tag{21}$$

$$\boldsymbol{u}_w = \begin{bmatrix} -\eta_{10} \mathrm{D}_t^{-\beta} s_1 - k_1 \mathrm{sgn}(s_1) \\ -\eta_{20} \mathrm{D}_t^{-\beta} s_2 - k_2 \mathrm{sgn}(s_2) \end{bmatrix} \tag{22}$$

$$\boldsymbol{\Lambda} = \begin{bmatrix} \hat{\alpha}_1 & 0 \\ 0 & \hat{\alpha}_2 \end{bmatrix} \tag{23}$$

In this formulation, $\hat{\alpha}_1$ and $\hat{\alpha}_2$ are the estimated parameters provided by adjustment mechanism in the closed loop system. Specifically, their dynamics are given as follows:

$$\begin{cases} \dot{\hat{\alpha}}_1 = -\gamma_1 s_1 \dfrac{1}{mK_M} \left[\dfrac{(C_1 - C_2)}{V} w + \dfrac{(C_1 L_{\mathrm{c}} - C_2 L_{\mathrm{e}})}{V} q + C_1 \delta_{\mathrm{e}} + C_2 \delta_{\mathrm{c}} \right] \\ \dot{\hat{\alpha}}_2 = -\gamma_2 s_2 \dfrac{1}{mK_\theta} \left[\dfrac{(-C_1 L_{\mathrm{c}} + C_2 L_{\mathrm{e}})}{V} w + \dfrac{\left(C_1 L_{\mathrm{c}}^2 - C_2 L_{\mathrm{e}}^2\right)}{V} q - C_1 L_{\mathrm{c}} \delta_{\mathrm{e}} + C_2 L_{\mathrm{e}} \delta_{\mathrm{c}} \right] \end{cases} \tag{24}$$

In this controller, $\boldsymbol{\Lambda}$ is the vector of the update terms by adaptive law corresponding to the variations of the vehicle payload. Consequently, the AFOSMC scheme in Eq. (19) can drive the uncertain vehicle dynamics in Eq. (1) to the sliding surface under appropriate control parameters as stated in Theorem 1.

Theorem 1. Consider the uncertain vehicle dynamics in Eq. (18). If some positive control parameters (η_1, η_2) are properly selected, then the AFOSMC algorithm in Eq. (19) guarantees the rate of convergence of the perturbed dynamical system in Eq. (1) to the sliding surface described in Eq. (17).

Proof. First, a Lyapunov function candidate is selected as:

$$\bar{V}(t, s) = V_1 + V_2, \tag{25}$$

where

$$V_1 = \frac{1}{2} s_1^2 + \frac{\tilde{\alpha}_1^2}{2\gamma_1 \alpha_1},\ V_2 = \frac{1}{2} s_2^2 + \frac{\tilde{\alpha}_2^2}{2\gamma_2 \alpha_2}. \tag{26}$$

This is an energy-like function with ensuring positive definite ($\bar{V} > 0$). The time derivative of this function becomes

$$\dot{\bar{V}} = s_1 \dot{s}_1 + s_2 \dot{s}_2 + \frac{\tilde{\alpha}_1 \dot{\tilde{\alpha}}_1}{\gamma_1 \alpha_1} + \frac{\tilde{\alpha}_2 \dot{\tilde{\alpha}}_2}{\gamma_2 \alpha_2}. \tag{27}$$

By applying the fractional calculus, the time derivative of the Lyapunov function can be written in the following forms:

$$\begin{cases} \dot{V}_1 = s_1 \left({}_0\mathrm{D}_t^{2+\beta} e_1(t) + \lambda_1 \dot{e}_1 \right) + \dfrac{\tilde{\alpha}_1 \dot{\tilde{\alpha}}_1}{\gamma_1 \alpha_1} = \\ \qquad s_1 \left({}_0\mathrm{D}_t^{\beta} \ddot{e}_1(t) + \lambda_1 \dot{e}_1 \right) + \dfrac{\tilde{\alpha}_1 \dot{\tilde{\alpha}}_1}{\gamma_1 \alpha_1} \\ \dot{V}_2 = s_2 \left({}_0\mathrm{D}_t^{2+\beta} e_2(t) + \lambda_2 \dot{e}_2 \right) + \dfrac{\tilde{\alpha}_2 \dot{\tilde{\alpha}}_2}{\gamma_2 \alpha_2} = \\ \qquad s_2 \left({}_0\mathrm{D}_t^{\beta} \ddot{e}_2(t) + \lambda_2 \dot{e}_2 \right) + \dfrac{\tilde{\alpha}_2 \dot{\tilde{\alpha}}_2}{\gamma_2 \alpha_2} \end{cases} \tag{28}$$

Then it can be described by,

$$\begin{cases} \dot{V}_1 = s_1 \left[{}_0\mathrm{D}_t^{\beta} \left(\dfrac{C_1 - C_2}{mK_M V} w + \dfrac{C_1 L_{\mathrm{c}} - C_2 L_{\mathrm{e}}}{mK_M V} q + \dfrac{C_1}{mK_M} u_1 + \dfrac{C_2}{mK_M} u_2 + g - Vq - \ddot{z}_{\mathrm{d}} \right) + \lambda_1 \dot{e}_1 \right] + \dfrac{\tilde{\alpha}_1 \dot{\tilde{\alpha}}_1}{\gamma_1 \alpha_1} \\ \dot{V}_2 = s_2 \left[{}_0\mathrm{D}_t^{\beta} \left(\dfrac{-C_1 L_{\mathrm{c}} + C_2 L_{\mathrm{e}}}{mK_\theta V} w + \dfrac{C_1 L_{\mathrm{c}}^2 - C_2 L_{\mathrm{e}}^2}{mK_\theta V} q - \dfrac{C_1 L_{\mathrm{c}}}{mK_\theta} u_1 - \dfrac{C_2 L_{\mathrm{e}}}{mK_\theta} u_2 - \ddot{\theta}_{\mathrm{d}} \right) + \lambda_2 \dot{e}_2 \right] + \dfrac{\tilde{\alpha}_2 \dot{\tilde{\alpha}}_2}{\gamma_2 \alpha_2} \end{cases} \tag{29}$$

Suppose that the nominal mass of vehicle is given by M, in which the corresponding nominal relative density is described by m. The real relative density is given by $\hat{m}$ which can be estimated by using two controlled channels as $\hat{m}_1 = \alpha_1 m$ and $\hat{m}_2 = \alpha_2 m$, where α_1 and α_2 are positive constants ($\in \Re^+$). With the updated values of relative density, Eq. (29) further becomes,

$$\begin{cases} \dot{V}_1 = s_1 \left[{}_0\mathrm{D}_t^{\beta} \left(\dfrac{\alpha_1 (C_1 - C_2)}{\hat{m}_1 K_M V} w + \dfrac{\alpha_1 (C_1 L_{\mathrm{c}} - C_2 L_{\mathrm{e}})}{\hat{m}_1 K_M V} q + \dfrac{\alpha_1 C_1}{\hat{m}_1 K_M} u_1 + \dfrac{\alpha_1 C_2}{\hat{m}_1 K_M} u_2 + g - Vq - \ddot{z}_{\mathrm{d}} \right) + \lambda_1 \dot{e}_1 \right] + \dfrac{\tilde{\alpha}_1 \dot{\tilde{\alpha}}_1}{\gamma_1 \alpha_1} \\ \dot{V}_2 = s_2 \left[{}_0\mathrm{D}_t^{\beta} \left(\dfrac{\alpha_2 (-C_1 L_{\mathrm{c}} + C_2 L_{\mathrm{e}})}{\hat{m}_2 K_\theta V} w + \dfrac{\alpha_2 \left(C_1 L_{\mathrm{c}}^2 - C_2 L_{\mathrm{e}}^2\right)}{\hat{m}_2 K_\theta V} q - \dfrac{\alpha_2 C_1 L_{\mathrm{c}}}{\hat{m}_2 K_\theta} u_1 - \dfrac{\alpha_2 C_2 L_{\mathrm{e}}}{\hat{m}_2 K_\theta} u_2 - \ddot{\theta}_{\mathrm{d}} \right) + \lambda_2 \dot{e}_2 \right] + \dfrac{\tilde{\alpha}_2 \dot{\tilde{\alpha}}_2}{\gamma_2 \alpha_2} \end{cases} \tag{30}$$

In order to obtain the optimal parameters, some parameters (α_1, α_2) are replaced by their estimations ($\hat{\alpha}_1$, $\hat{\alpha}_2$) utilizing adjustment mechanism, where $\hat{\alpha}_1 = \alpha_1 + \tilde{\alpha}_1$ and

$\hat{\alpha}_2 = \alpha_2 + \tilde{\alpha}_2$. Then Eq. (30) can be rewritten as follows:

$$\begin{cases} \dot{V}_1 = s_1\left\{{}_0\mathrm{D}_t^{\beta}\left[\dfrac{\tilde{\alpha}_1}{\alpha_1}\left(\dfrac{(C_1-C_2)}{mK_MV}w+\dfrac{(C_1L_c-C_2L_e)}{mK_MV}q+\dfrac{C_1}{mK_M}u_1+\dfrac{C_2}{mK_M}u_2\right)\dfrac{(C_1-C_2)}{mK_MV}w+\dfrac{(C_1L_c-C_2L_e)}{mK_MV}q+\dfrac{C_1}{mK_M}u_1+\dfrac{C_2}{mK_M}u_2+g-Vq-\ddot{Z}_d\right]+\lambda_1\dot{e}_1\right\}+\dfrac{\tilde{\alpha}_1\dot{\tilde{\alpha}}_1}{\gamma_1\alpha_1} \\ \dot{V}_2 = s_2\left\{{}_0\mathrm{D}_t^{\beta}\left[\dfrac{\tilde{\alpha}_2}{\alpha_2}\left(\dfrac{(-C_1L_c+C_2L_e)}{mK_\theta V}w+\dfrac{\left(C_1L_c^2-C_2L_e^2\right)}{mK_\theta V}q-\dfrac{C_1L_c}{mK_\theta}u_1-\dfrac{C_2L_e}{mK_\theta}u_2\right)\dfrac{(-C_1L_c+C_2L_e)}{mK_\theta V}w+\dfrac{\left(C_1L_c^2-C_2L_e^2\right)}{mK_\theta V}q-\dfrac{C_1L_c}{mK_\theta}u_1-\dfrac{C_2L_e}{mK_\theta}u_2-\ddot{\theta}_d\right]+\lambda_2\dot{e}_2\right\}+\dfrac{\tilde{\alpha}_2\dot{\tilde{\alpha}}_2}{\gamma_2\alpha_2} \end{cases} \tag{31}$$

$$\begin{cases} \dot{V}_1 = s_1\left\{{}_0\mathrm{D}_t^{\beta}\left[\dfrac{\tilde{\alpha}_1}{\alpha_1}\left(\dfrac{C_1-C_2}{mK_MV}w+\dfrac{C_1L_c-C_2L_e}{mK_MV}q\right)+\dfrac{\tilde{\alpha}_1}{\alpha_1}\left(\dfrac{C_1}{mK_M}\delta_e+\dfrac{C_2}{mK_M}\delta_c\right)-\lambda_{10}\mathrm{D}_t^{1-\beta}e_1-\eta_{10}\mathrm{D}_t^{-\beta}s_1-k_1\mathrm{sgn}(s_1)\right]+\lambda_1\dot{e}_1\right\}+\dfrac{\tilde{\alpha}_1\dot{\tilde{\alpha}}_1}{\gamma_1\alpha_1} \\ \dot{V}_2 = s_2\left\{{}_0\mathrm{D}_t^{\beta}\left[\dfrac{\tilde{\alpha}_2}{\alpha_2}\left(\dfrac{-C_1L_c+C_2L_e}{mK_\theta V}w+\dfrac{C_1L_c^2-C_2L_e^2}{mK_\theta V}q\right)-\dfrac{\tilde{\alpha}_2}{\alpha_2}\left(\dfrac{C_1}{mK_\theta}L_c\delta_e+\dfrac{C_2}{mK_\theta}L_e\delta_c\right)-\lambda_{20}\mathrm{D}_t^{1-\beta}e_2-\eta_{20}D_t^{-\beta}s_2-k_2\mathrm{sgn}(s_2)\right]+\lambda_2\dot{e}_2\right\}+\dfrac{\tilde{\alpha}_2\dot{\tilde{\alpha}}_2}{\gamma_2\alpha_2} \end{cases} \tag{32}$$

The updated dynamics of the correcting factors $\hat{\alpha}_1$ and $\hat{\alpha}_2$ are also modified with respect to the sliding surfaces and payload changes. If the adaptive law in Eq. (24) is employed for their derivatives, then the constituents of the Lyapunov function can be obtained by,

$$\begin{cases} \dot{V}_1 = -\eta_1 s_1^2 \leqslant 0 \\ \dot{V}_2 = -\eta_2 s_2^2 \leqslant 0 \end{cases} \tag{33}$$

By checking Theorem 1, it can be realized that $\dot{\tilde{V}} = \dot{V}_1 + \dot{V}_2 \leqslant 0$ (negative semi-definite). Then the stability with convergence to the sliding surfaces will be accomplished.

It can be seen that the AFOSMC has the same structure as the STWSMC but AFOSMC scheme has more flexible structure due to fractional orders of the sliding variables and the adaptive parameters. Hence AFOSMC strategy effectively deals with the disturbances such as the payload variations. The comparative results between AFOSMC and STWSMC will be shown in the numerical simulation, where the graphical results, as well as some performance criteria will be provided for evaluation.

4 Simulation results and discussions

The numerical simulations have been conducted to validate the proposed vehicle design methods. Since the pitch angle changes will finally affect the vehicle depth which defines its vertical trajectory, the maneuvering performance related to the vertical plane is only demonstrated in numerical simulation. By comparing with the other results on supercavitating vehicle, the control system must comply with the following strict requirements:

• Settling time less than 0.4 s for a step reference of 3 m;

• No overshoot with a short rise time;

• Smaller than 5% steady-state error when the vehicle mass changes;

• Low or no chattering of actuating signals in the steady state;

• Disturbance attenuation guaranteeing at least 70%.

With the design specifications mentioned above, the AFOSMC algorithm has been successfully implemented with some parameters selected as follows: $\gamma_1 = 0.01$, $\gamma_2 = 0.005$, $\lambda_1 = 16$, $\lambda_2 = 20$, $\eta_1 = 12$, and $\eta_2 = 10$. Firstly, the transient response for a step input reference of 3 m depth is illustrated in Fig. 3. The depth response is depicted in Fig. 3a and the other states in the dive plane are shown in Figs. 3c and 3d. It can be observed from the results that the vehicle responses guarantee very fast and precise diving with settling time less than 0.4 s, and no overshoot with zero error at steady state. The other corresponding states pose some fluctuations during transient period and become asymptotically stable afterward. For performance comparison, the well-known STWSMC strategy is also simulated and illustrated in Fig. 3a as the dashed line. It can be seen that the proposed AFOSMC clearly outperforms its typical integer-order counterpart of STWSMC with offering superior results in terms of time-domain responses.

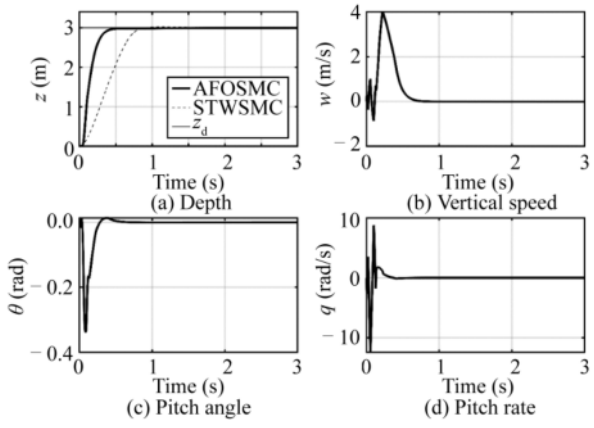

Fig. 3. Transient responses of the controlled vehicle system: (a) depth, (b) vertical speed, (c) pitch angle, and (d) pitch rate.

As illustrated in Fig. 4, it can be easily observed that the actuating signals of the proposed AFOSMC are more active

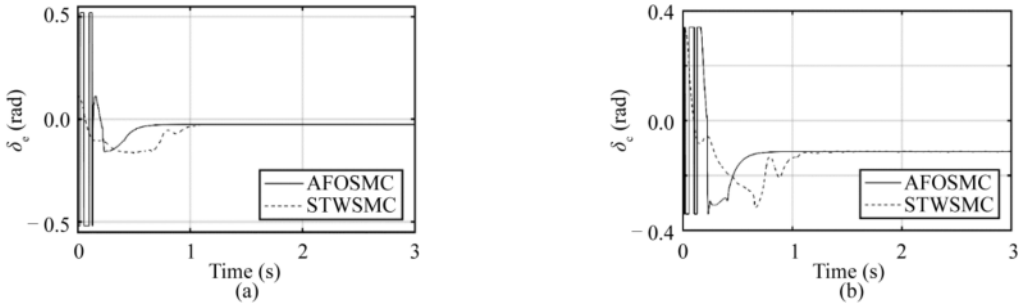

Fig. 4. Control actions corresponding to the step responses.

than STWSMC in the transient time. The AFOSMC control actions are alternatively changing angles of the actuators up to their saturated values, to drive the vehicle tracking the reference as soon as possible. In fact, one can make the control signals of the STWSMC more active by increasing the control gains to obtain a faster response. However, this will lead to boosting the existing overshoot as shown in Fig. 3a. Note that for high speeds of the supercavitating vehicle, a little overshoot and oscillation may result in unfortunate accidents and catastrophic system failures. Furthermore, the saturations are harmful to the actuators if they occur often. However, actuator saturation in very short transient time to achieve fast response is not a serious problem but is an evidence for the activeness of the proposed AFOSMC.

The high flexibility with performance superiority of the proposed AFOSMC is accomplished by fractional order of $\beta = 0.05$. In fact, different levels of vehicle performance can be achieved by selecting different values of the fractional orders. It is worth noting that the fractional-order β provides one more degree of freedom to tune the vehicle controller. Fig. 5 shows the system performance of the AFOSMC scheme with different fractional orders. It can be observed that the lower order scheme starts to produce overshoots while the higher orders will yield slow responses.

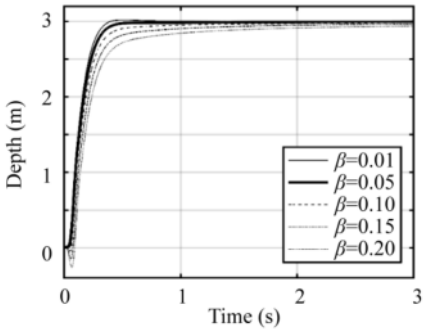

Fig. 5. Transient responses of the controlled system with fractional orders.

The nonlinear planing force is one of the challenging issues for vehicle controller design. As stated earlier, the state-feedback controller could not effectively eliminate the planing forces that lead to periodic motion (Dzielski and Kurdila, 2003; Phuc et al., 2020). However, the proposed AFOSMC can completely reject the planing forces occurring during turning maneuvers, as proven in Fig. 6. The proposed AFOSMC is an efficient approach for dealing with the tail-slapped planing force, which results in the smooth vehicle motions with safety as illustrated in Fig. 3.

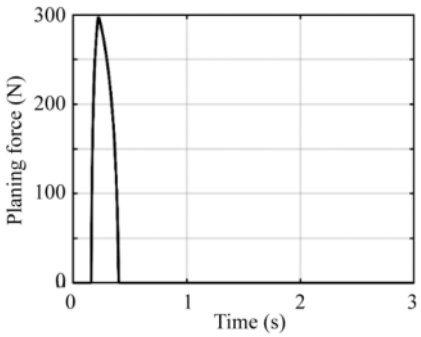

Fig. 6. Controlled planing force due to the step response.

The major goal of this research is to design a robust controller that can effectively cope with vehicle payload mass changes. To verify this ability of the proposed controller, the vehicle mass is assumed to be changed randomly around its nominal value during maneuvers, as in Fig. 7b. It can be observed from Fig. 7a that at the transient time period, the STWSMC produced a high overshoot in its depth response due to the mass change while the AFOSMC still guarantees its best response. In the steady-states, at time =5 s and time =7 s, due to big mass changes, there are some fluctuations in both controllers. However, the variations in the depth response of the AFOSMC are not noticeable compared with that of the STWSMC with its corresponding control actions as shown in Fig. 8. From the magnified subfigures, one can interestingly see that the AFOSMC can act on mass changes more drastically than the STWSMC, by exploiting the maximized ability of the elevators and cavitator to quickly stabilize the vehicle motions.

Note that the adaptation mechanism in the proposed AFOSMC mainly deals with the payload changes to improve the dynamical response. The updated law for correcting components $\hat{\alpha}_1$ and $\hat{\alpha}_2$ in this algorithm will adjust their

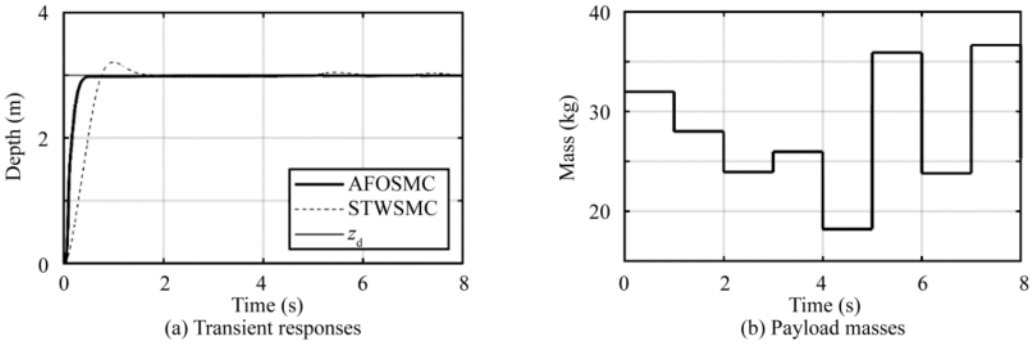

Fig. 7. Time histories of the controlled systems due to payload mass changes: (a) transient responses, and (b) payload masses.

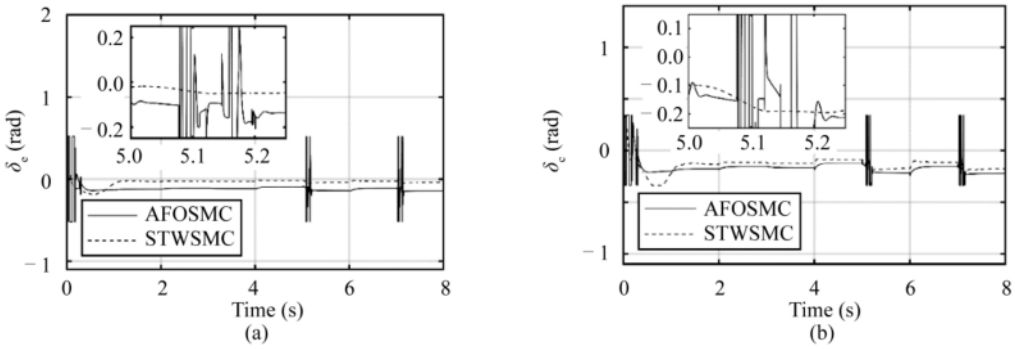

Fig. 8. Control actions under payload mass changes.

values which respect to the current value of vehicle mass and corresponding sliding variables. The updated parameters of these correcting actions can be illustrated in Fig. 9. In this figure, their values have big variations during the transient time when the sliding variables are far from zero and keep the fixed values in the steady state. The magnified subfigures at time =5 s show that the adjusted parameters ($\hat{\alpha}_1$ and $\hat{\alpha}_2$) have slightly updated their values to adapt to the new payloads. Although the adaptations are slight, they play very important role in how to improve the robustness for the complete control algorithm.

Next, the controlled system should be designed to guarantee the ability of disturbance elimination. In this simulation, an external disturbance has been introduced at time = 3 s. The disturbance may be a disturbing force caused by an undersea current which tends to push the vehicle away from its normal trajectory. As shown in Fig. 10, it can be observed that both controllers have eliminated disturbance effect in different levels. The AFOSMC can reject more than 90% of disturbance effect compared with 40% of the STWSMC. One can realize that the controlled vehicle system by AFOSMC has higher robustness and insensitive to external disturbance. The corresponding control actions of both controllers are depicted in Fig. 11, where the AFOSMC are more active than the STWSMC in reacting to the disturbance inputs.

In addition to the graphical illustrations, the comparison between the control performances is also provided by using time integral criteria. Table 1 shows the performance of the two controllers in all three simulations including the normal

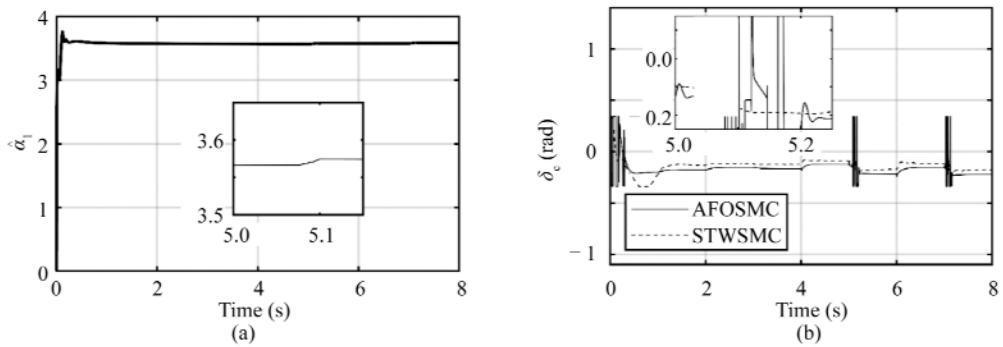

Fig. 9. Parameter convergence adjusted by adaptive law.

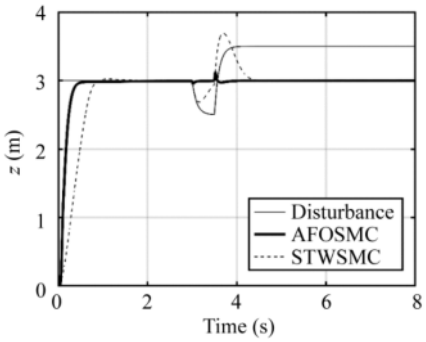

Fig. 10. Depth responses to the external disturbances.

case, the case with changing mass, and the case with an external disturbance. The performance indices include the integral of the absolute value of the square error (IAE) and the integral of the square error (ISE). The smaller values of these indices of AFOSMC compared with those of STWSMC in all the cases confirm the predominance of the proposed control algorithm which provides faster responses and better regulations against uncertainties.

In summary, the simulation results show that the proposed AFOSMC strategy satisfies all the required criteria and outperforms the STWSMC as well as the other controllers existing in the literature.

5 Conclusions

Underwater vehicles can achieve high speed by exploiting supercavitation technology. Supercavitating vehicle is traveling at extremely high speeds against parameter variations with undersea disturbances. It can be a next-generation marine vehicle capable of changing the paradigm of modern underwater vehicle. The robust control synthesis of the supercavitating vehicle is one of the most challenges due to its structure and maneuver conditions. This paper has investigated the dynamical behaviors of the underwater vehicle model, especially under the effects of the payload changes with disturbances on vehicle stability. The study shows that:

(1) There are some ranges of the vehicle mass where bifurcation occurs and suggests that the vehicle mass should be designed in the range of 25−27 kg to ensure better stability.

(2) Based on the bifurcation analysis, a comparative study of the efficacy of the control algorithms is presented to solve the optimization problem. Specifically, a novel AFOSMC scheme has been introduced to guarantee the dynamic performance with the ability to cope with the nonlinear planing force, payload mass changes, and external disturbance to robustly maneuver and stabilize the underwater vehicles.

(3) The extensive simulation results show that the proposed fractional order controller offers the fastest response with accuracy and stability, demonstrated by the comparison study with the STWSMC and by checking the performances of other controllers in the literature. The dive plane responses realized by the proposed controller are also very smooth, and the control system especially guarantees speedy responses with accuracy without overshoot.

(3) By introducing the update algorithm for correcting factors in the adaptive terms, the proposed controller becomes more effective in dealing with the payload mass changes and external disturbances. The proposed controlled system is almost insensitive to the large payload variations and extreme disturbances, which cannot be handled by the integer-order counterpart of STWSMC.

(4) By exploiting the fractional calculus, more control freedoms with design flexibility can be gained so that system designers can easily tune the vehicle controllers satisfying very strict design criteria against extreme undersea environments.

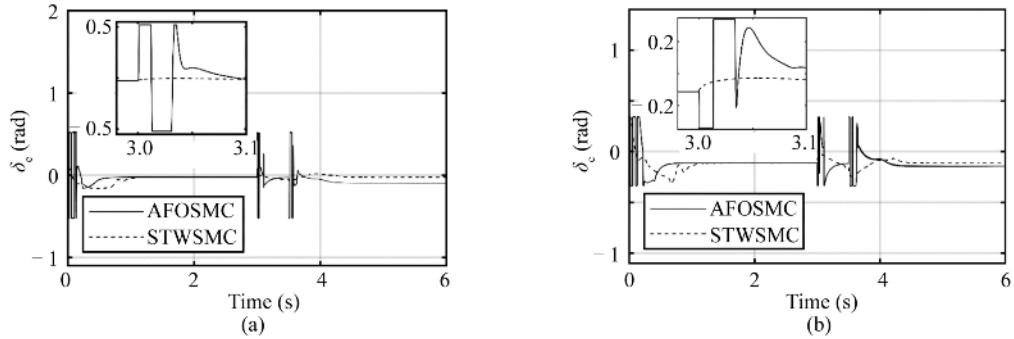

Fig. 11. Active control actions under external disturbances.

Table 1 Comparison of control schemes using performance criteria

Criterion	AFOSMC (Normal)	STWSMC (Normal)	AFOSMC (Mass changed)	STWSMC (Mass changed)	AFOSMC (External disturbance)	STWSMC (External disturbance)
IAE	0.4794	1.1846	0.5161	1.3415	0.5144	1.5867
ISE	0.9475	2.4946	0.9480	2.6109	0.9492	2.6713

References

Anukul, G., 2005. *Robust Control of Supercavitating Vehicles in the Presence of Dynamic and Uncertain Cavity*, Ph.D. Thesis, University of Florida, Gainesville, FL.

Dzielski, J. and Kurdila, A., 2003. A benchmark control problem for supercavitating vehicles and an initial investigation of solutions, *Journal of Vibration and Control*, 9(7), 791–804.

Fan, H., Zhang, Y.W. and Wang, X.N., 2011. Longitudinal dynamics modeling and MPC strategy for high-speed supercavitating vehicles, *Proceedings of 2011 International Conference on Electric Information and Control Engineering*, IEEE, Wuhan, China, pp. 5947–5950.

Fan, J.L., Zhao, G.L. and Zhao, X.H., 2010. Adaptive sliding mode control of supercavitating vehicles, *Journal of Huazhong University of Science and Technology* (*Nature Science*), 38(1), 109–113. (in Chinese)

Han, Y.T., Bi, X.J. and Bai, T., 2010. Dynamic inversion control based on backstepping for underwater high-speed vehicle, *Proceedings of the 2010 8th World Congress on Intelligent Control and Automation* (*WCICA*), IEEE, Jinan, China, pp. 3868–3871.

Han, Y.T. and Geng, R.G., 2012. Active disturbance rejection control of underwater high-speed vehicle, *Proceeding of the 2012 IEEE International Conference on Automation and Logistics*, IEEE Zhengzhou, China, pp. 550–553.

Jafarian, A. and Pishevar, A., 2016. Numerical simulation of steady supercavitating flows, *Journal of Applied Fluid Mechanics*, 9(6), 2981–2992.

Kirschner, I.N., Kring, D.C., Stokes, A.W., Fine, N.E. and Uhlman, J.S., 2002. Control strategies for supercavitating vehicles, *Journal of Vibration and Control*, 8(2), 219–242.

Kulkarni, S.S. and Pratap, R., 2000. Studies on the dynamics of a supercavitating projectile, *Applied Mathematical Modelling*, 24(2), 113–129.

Lin, G.J., Balachandran, B. and Abed, E., 2006. Nonlinear dynamics and control of supercavitating bodies, *Proceedings of the AIAA Guidance*, *Navigation*, *and Control Conference and Exhibit*, AIAA, Keystone, Colorado, USA, pp. 3151–3164.

Lin, G.J., Balachandran, B. and Abed, E.H., 2008. Dynamics and control of supercavitating vehicles, *Journal of Dynamic Systems*, *Measurement*, *and Control*, 130(2), 021003.

Lv, R., Wei, Y.J., Zhang, J.Z., Yu, K.P. and Wang J.H., 2011. Sliding mode control of supercavitating vehicles in the vertical plane using guaranteed cost theory, *High Technology Letter*, 17(2), 186–190.

Lv, R., Yu, K.P., Wei, Y.J., Zhang, J.Z. and Wang, J.H., 2010. Adaptive sliding mode controller design for a supercavitating vehicle, *Proceedings of the 3rd International Symposium on Systems and Control in Aeronautics and Astronautics*, IEEE, Harbin, China, pp. 885–889.

Mao, X.F. and Wang Q., 2009. Nonlinear control design for a supercavitating vehicle, *IEEE Transactions on Control Systems Technology*, 17(4), 816–832.

Mao, X.F. and Wang, Q., 2015. Adaptive control design for a supercavitating vehicle model based on fin force parameter estimation, *Journal of Vibration and Control*, 21(6), 1220–1233.

May, A. 1975. *Water Entry and the Cavity-Running Behavior of Missiles*, NAVSEA Hydroballistics Advisory Committee, Silver Spring, MD, USA, pp. 75–82.

Oustaloup, A., Levron, F., Mathieu, B. and Nanot, F.M., 2000b. Frequency-band complex noninteger differentiator: characterization and synthesis, *IEEE Transactions on Circuits and Systems I*: *Fundamental Theory and Applications*, 47(1), 5–39.

Oustaloup, A., Melchior, P., Lanusse, P., Cois, O. and Dancla, F., 2000a. The CRONE toolbox for Matlab, *CACSD Conference Proceedings IEEE International Symposium on Computer-Aided Control System Design*, IEEE, Anchorage, AK, USA, pp. 190–195.

Phuc, B.D.H., Lee, S.D., You, S.S. and Rathore, N.S., 2020. Nonlinear robust control of high-speed supercavitating vehicle in the vertical plane, *Proceedings of the Institution of Mechanical Engineers*, *Part M*: *Journal of Engineering for the Maritime Environment*, 234(2), 510–519.

Phuc, B.D.H., You, S.S., Rathore, N.S. and Kim, H.S., 2019. Dynamical analysis and robust control for dive plane of supercavitating vehicles, *Applied Ocean Research*, 84, 259–267.

Podlubny, I., 1999. Fractional-order systems and $PI^{\lambda}D^{\mu}$-controllers, *IEEE Transactions on Automatic Control*, 44(1), 208–214.

Podlubny, I., Dorcák, L. and Kostial, I., 1997. On fractional derivatives, fractional-order dynamic systems and $PI^{\lambda}D^{\mu}$-controllers, *Proceedings of the 36th IEEE Conference on Decision and Control*, IEEE, San Diego, CA, USA, pp. 4985–4990.

Rand, R., Pratap, R., Ramani, D., Cipolla, J. and Kirschner, I., 1997. Impact dynamics of a supercavitating underwater projectile, *Proceedings of the 1997 ASME Design Engineering Technical Conferences*, *16th Biennial Conference on Mechanical Vibration and Noise*, Sacramento, CA, USA, pp. 1–11.

Utkin, V.I., 2008. Sliding mode control: Mathematical tools, design and applications, *Nonlinear and Optimal Control Theory*, , 289–347.

Vanek, B., Balas, G.J. and Arndt, R.E.A., 2010. Linear, parameter-varying control of a supercavitating vehicle, *Control Engineering Practice*, 18(9), 1003–1012.

Vanek, B., Bokor, J., Balas, G.J. and Arndt, G.E.A., 2007. Longitudinal motion control of a high-speed supercavitation vehicle, *Journal of Vibration and Control*, 13(2), 159–184.

Xue, D.Y. and Chen, Y.Q., 2002. A comparative introduction of four fractional order controllers, *Proceedings of the 4th World Congress on Intelligent Control and Automation*, IEEE, Shanghai, China, pp. 3228–3235.

You, S.S., Choi, H.S., Kim, H.S. and Park, H.I., 2011. Autopilot control synthesis for path tracking maneuvers of underwater vehicles, *China Ocean Engineering*, 25(2), 237–249.

Zhao, L., Wang, P., Sun, C.Y. and Song, B.W., 2019. Modeling and motion simulation for a flying-wing underwater glider with a symmetrical airfoil, *China Ocean Engineering*, 33(3), 322–332.

Zhao, X.H., Duan, G.R. and Sun, Y., 2011. Complex control system design for time delay supercavitating vehicle, *Engineering Mechanics*, 28(9), 234–239. (in Chinese)

Zhao, X.H., Sun, Y., Zhao, G.L. and Fan, J.L., 2014. μ-synthesis robust controller design for the supercavitating vehicle based on the BTT strategy, *Ocean Engineering*, 88, 280–288.

Appendix A

The detail elements of vehicle system matrices (***A***, ***B***, and ***F***) in Eqs. (3) and (4) are calculated as follows:

$$a_{22}=\frac{C_1-C_2}{MV},\ a_{24}=\frac{C_1L_c-C_2L_e}{MV},$$

$$a_{42}=\frac{-C_1L_c+C_2L_e}{I_{yy}V},\ a_{44}=\frac{C_1L_c^2-C_2L_e^2}{I_{yy}V};\tag{A1}$$

$$b_{21}=\frac{C_1}{M},\ b_{22}=\frac{C_2}{M},$$

$$b_{41}=-\frac{C_1}{I_{yy}}L_c,\ b_{42}=-\frac{C_2}{I_{yy}}L_e;\tag{A2}$$

$$d_2=\frac{C_p}{M},\ d_4=-\frac{C_p}{I_{yy}},\tag{A3}$$

where the intermediate parameters (C_1, C_2, and C_p) are specifically described as:

$$C_1=0.5\pi\rho R_n^2V^2C_x,$$

$$C_2=0.5\pi\rho R_n^2V^2C_xn,$$

$$C_p=\pi\rho R^2V^2.\tag{A4}$$

The nonlinear planing force is calculated as:

$$F_p=-V^2\left[1-\left(\frac{R_c-R}{h'R+R_c-R}\right)^2\right]\frac{1+h'}{1+2h'}\bar{\alpha},\tag{A5}$$

where the diameter of the cavity at the planing location is R_c. This diameter can be computed using

$$R_c=R_n\sqrt{0.82\frac{1+\sigma}{\sigma}K_2}.\tag{A6}$$

In addition, h' is the immersion depth given by

$$h'=\begin{cases}0, & \dfrac{R_c-R}{R}>\dfrac{L|w|}{RV}\\ \dfrac{L|w|}{RV}-\dfrac{R_c-R}{R}, & \text{otherwise}\end{cases}\tag{A7}$$

Moreover, α is the angle of attack defined as:

$$\bar{\alpha}=\begin{cases}\dfrac{w-\dot{R}_c}{V}, & \dfrac{w}{V}>0\\ \dfrac{w+\dot{R}_c}{V}, & \text{otherwise}\end{cases}\tag{A8}$$

where the contraction rate of the cavity R_c is calculated by

$$\dot{R}_c=\frac{-1.176\sqrt{\left(0.82\dfrac{1+\sigma}{\sigma}\right)}V\left(1-\dfrac{4.5\sigma}{1+\sigma}\right)K_1{}^{23/17}}{K_2\left(\dfrac{1.92}{\sigma}-3\right)}\tag{A9}$$

provided that the following expressions should hold:

$$K_1=\frac{L}{R_n\left(\dfrac{1.92}{\sigma}-3\right)}-1;$$

$$K_2=\sqrt{1-\left(1-\frac{4.5\sigma}{1+\sigma}\right)K_1{}^{40/17}}.\tag{A10}$$

Appendix B

Table 2 Model parameters of the underwater vehicle system

Parameter	Value
C_{x0}	0.82
g	9.81 m/s^2
L	1.18 m
m	2
n	0.5
R_n	0.0191 m
R	0.0508 m
V	75 m/s
σ	0.03